*Nano Research* 2018, 11(2): 864–873
https://doi.org/10.1007/s12274-017-1697-x
**Research Article**
ISSN 1998-0124
CN 11-5974/O4

# Atomic and electronic structure of Si dangling bonds in quasi-free-standing monolayer graphene

Yuya Murata[1], Tommaso Cavallucci[1], Valentina Tozzini[1], Niko Pavliček[2], Leo Gross[2], Gerhard Meyer[2], Makoto Takamura[3], Hiroki Hibino[3,†], Fabio Beltram[1], and Stefan Heun[1] (✉)

[1] *NEST, Istituto Nanoscienze-CNR and Scuola Normale Superiore, Piazza San Silvestro 12, 56127 Pisa, Italy*
[2] *IBM Research-Zurich, Säumerstrasse 4, 8803 Rüschlikon, Switzerland*
[3] *NTT Basic Research Laboratories, 3-1 Morinosato Wakamiya, Atsugi, Kanagawa 243-0198, Japan*
[†] *Present address: Kwansei Gakuin University, 2-1 Gakuen, Sanda, Hyogo 669-1337, Japan*

**Received:** 12 April 2017
**Revised:** 29 May 2017
**Accepted:** 1 June 2017



**KEYWORDS**
quasi-free-standing monolayer graphene,
hydrogen intercalation,
carrier mobility,
scanning tunneling microscopy,
scanning tunneling spectroscopy,
atomic force microscopy,
density functional theory

## ABSTRACT

Si dangling bonds at the interface of quasi-free-standing monolayer graphene (QFMLG) are known to act as scattering centers that can severely affect carrier mobility. Herein, we investigate the atomic and electronic structure of Si dangling bonds in QFMLG using low-temperature scanning tunneling microscopy/spectroscopy (STM/STS), atomic force microscopy (AFM), and density functional theory (DFT) calculations. Two types of defects with different contrast were observed on a flat graphene terrace by STM and AFM; in particular, their STM contrast varied with the bias voltage. Moreover, these defects showed characteristic STS peaks at different energies, 1.1 and 1.4 eV. The comparison of the experimental data with the DFT calculations indicates that the defects with STS peak energies of 1.1 and 1.4 eV consist of clusters of three and four Si dangling bonds, respectively. The relevance of the present results for the optimization of graphene synthesis is discussed.

## 1 Introduction

Graphene, a two-dimensional sheet of carbon atoms, is attracting considerable interest for applications in high-speed electronics, owing to its high carrier mobility [1]. The latter, however, can be severely reduced by scattering centers introduced by its supporting substrate. This issue is stimulating new investigations aimed at the development of synthesis methods that can minimize the graphene interaction with the substrate.

Address correspondence to stefan.heun@nano.cnr.it

Graphitization of a silicon carbide (SiC) surface represents a promising process for electronic applications, because graphene is grown directly on an insulating substrate, without a transfer process. In the first step of graphene synthesis on a SiC(0001) surface, a carbon layer, called buffer layer, is formed by annealing the SiC substrate in vacuum or in an inert-gas atmosphere, leading to sublimation of surface Si atoms from the substrate. Even though the buffer layer consists of a honeycomb structure of carbon atoms, it does not have the electronic properties of graphene, owing to the formation of covalent bonds with the substrate [2]. The buffer layer can be detached from the substrate and transformed to $sp^2$-hybridized carbon (graphene), either by further thermal decomposition of the SiC substrate underneath the buffer layer, or by intercalation of H atoms at the interface between buffer layer and substrate [3, 4]. The former approach results in the formation of epitaxial monolayer graphene (EMLG), whereas the latter produces quasi-free-standing monolayer graphene (QFMLG). The carrier mobility of QFMLG shows a weaker temperature dependence compared with EMLG [5]. This was attributed to the reduced interaction between carriers in QFMLG and substrate phonons. However, the carrier mobility in QFMLG (~ 6,600 $cm^2 \cdot V^{-1} \cdot s^{-1}$) [6] is lower than that in free-standing graphene, indicating the presence of residual carrier-scattering centers.

Based on photoelectron spectroscopy measurements, it was suggested that non-hydrogen terminated Si dangling bonds at the interface donate charge to graphene and act as charged scattering centers [7]. In a previous report, we analyzed the correlation between the morphology of QFMLG and the substrate temperature during H intercalation ($T_H$) [8]. Room-temperature scanning tunneling microscopy (STM) images of QFMLG samples formed at $T_H$ = 600 and 800 ℃ revealed depressions with a width of 1 nm on flat terraces. These depressions are distributed with the periodicity of the quasi-(6 × 6) reconstruction of the SiC(0001) surface, i.e., with the periodicity of the buffer layer. This suggests that the depressions correspond to the positions of Si dangling bonds at the interface, because theoretical studies reported that the hydrogenation energies of the Si sites located within the unit cell of a buffer layer model span a range of 1 eV [9]. The strong preference of H to bind to symmetric sites might in certain conditions lead to a symmetric location also for the last non-hydrogenated sites, i.e., for the possible residual H vacancies. It was also found that the density of the depressions observed on a QFMLG sample formed at $T_H$ = 1,000 ℃ is two orders of magnitude smaller than that of samples formed at $T_H$ = 600 and 800 ℃ [8]. As $T_H$ increases, the dissociation of $H_2$ molecules, the intercalation of H atoms, and their diffusion along the graphene–substrate interface are promoted, which leads to a better H intercalation, i.e., to the formation of lower amounts of Si dangling bonds [10]. A similar distribution of Si dangling bonds at the interface of quasi-free-standing bilayer graphene was reported by noncontact scanning nonlinear dielectric potentiometry [11]. However, the detailed structure of the Si dangling bonds and their interaction with graphene are still poorly understood.

In this work, the atomic and electronic structure of Si dangling bonds in QFMLG is investigated using low-temperature STM, atomic force microscopy (AFM), and density functional theory (DFT) calculations.

## 2 Experimental

The samples were prepared following the same procedure reported in Refs. [8, 12]. Briefly, a 4H-SiC(0001) substrate was initially cleaned by annealing in $H_2$ at 33 mbar and 1,500 ℃ for 5 min. A buffer layer was formed by annealing in Ar atmosphere at 800 mbar and 1,650 ℃ for 5 min. Finally, the sample was annealed in $H_2$ at 1,013 mbar and $T_H$ = 1,000 ℃ for 60 min for H intercalation. The sample was then mounted in an ultra-high vacuum chamber and annealed at 250 ℃ for 1 h and at 600 ℃ for 10 min. The resulting product was characterized by STM/AFM in a homebuilt combined STM/AFM device, operating under ultrahigh vacuum conditions (base pressure $p < 10^{-10}$ mbar) at a temperature of 5 K. The microscope is equipped with a qPlus sensor [13, 14] with an eigenfrequency $f_0$ = 31,034 Hz, a stiffness $k$ = 1,800 $N \cdot m^{-1}$, and a quality factor of the order of $10^5$. A bias voltage $V$ was applied to the sample. The AFM measurements were conducted in frequency-modulation mode [15] at an oscillation amplitude ($A$) of 50 pm. The STM images were obtained in constant-current mode, in which a feedback adjusts

the height of the tip above the surface so that the tunneling current is kept constant. Scanning tunneling spectroscopy (STS) measurements were performed after stabilizing the tip-sample distance at a bias voltage $V_{stab}$ and tunneling current $I_{stab}$. The AFM images were obtained in constant-height mode, in which the tip is scanned without a feedback parallel to the surface while the shift in the resonance frequency, $\Delta f$, is recorded, and the images are taken at distances for which $\Delta f$ increases (to less negative values) as the tip-sample distance decreases.

DFT calculations were performed with the Quantum ESPRESSO [16] (QE, version 5.3.0) code, with a previously tested setup [17] involving ultrasoft pseudopotentials [18] and the Perdew–Burke–Ernzerhof (PBE) exchange-correlation functional [19] with the van der Waals D2 correction scheme [20]. The supercell employed in the calculations had a $(\sqrt{31}\times\sqrt{31})$ R8.95° periodicity with respect to SiC (which is a good approximation to the quasi-(6 × 6) symmetry) and a (7 × 7) R21.787° periodicity with respect to graphene. This choice has the advantage of including a relative small number of atoms in the model system (284), thus allowing extensive calculations at the expense of only a 0.7° rotation of graphene with respect to SiC. The present simulation cell hosts a single H vacancy per unit cell, corresponding to the maximum vacancy concentration observed in the experiments. Further details about the calculation setup are provided in the Electronic Supplementary Material (ESM).

## 3 Results

Figures 1(a)–1(h) show STM images taken at various bias voltages around a 0.25 nm-deep void in the SiC substrate. The void may be formed by etching of the SiC substrate during H intercalation at 1,000 ˚C [8]. In the STM image of Fig. 1(a), taken at +1.5 V bias, two types of bright features with different contrast are observed on a flat terrace. The brighter and less bright features are labeled A and B, respectively. These features were consistently observed in various areas of the sample.

As shown in the ESM, a histogram of the heights associated with a total of 166 analyzed features shows two clear peaks at 0.07 and 0.13 nm, corresponding to

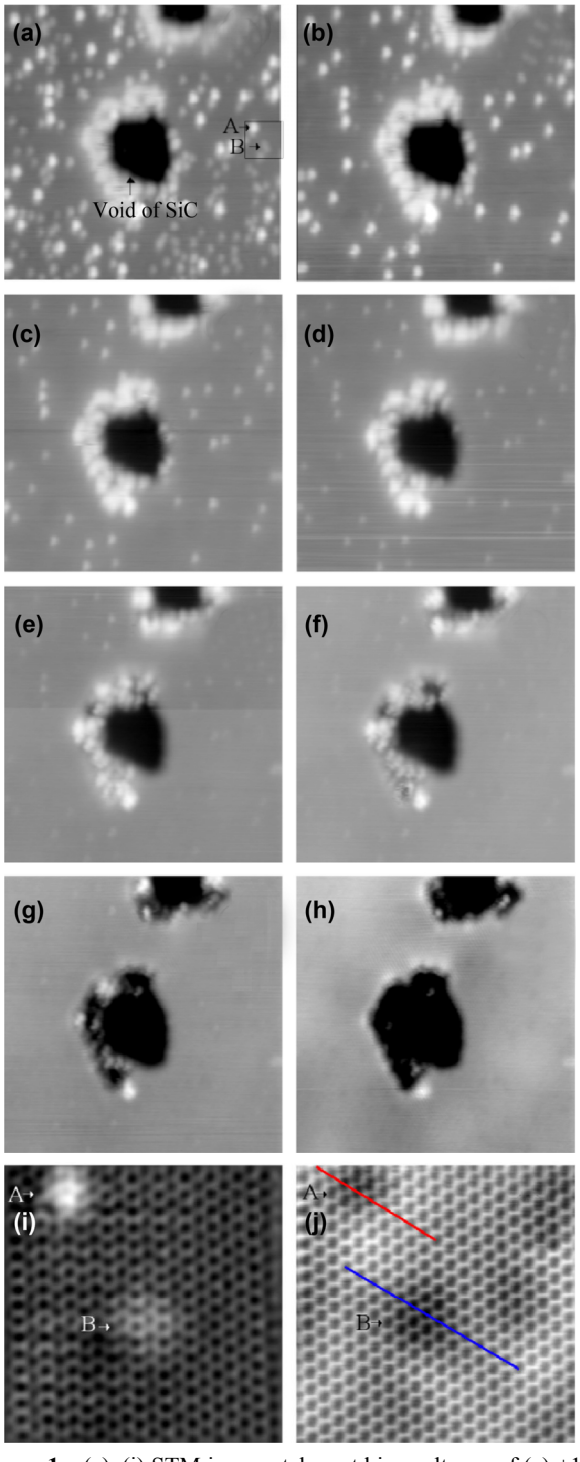


**Figure 1** (a)–(i) STM images taken at bias voltages of (a) +1.5, (b) +1.0, (c) +0.75, (d) +0.5, (e) +0.3, (f) +0.2, (g) +0.1, (h) –0.05, and (i) +0.1 V and tunneling currents of (a)–(h) 5 and (i) 20 pA. Image (i) corresponds to the area indicated by the square in (a). (j) Constant-height AFM image taken in the same area as (i). The color scale ranges from –62.6 Hz (black) to –52.3 Hz (white). The image sizes are 30 nm × 30 nm (a)–(h) and 4 nm × 4 nm (i) and (j). The images were taken at $T$ = 5 K. The features A and B discussed in the text are indicated by arrows in (a), (i), and (j).

features B and A, respectively, confirming that they represent two distinct groups of features. Figures 1(a)–1(h) show how the contrast of the A and B features changes with the bias voltage. The above-mentioned void observed in the SiC substrate was used as a reference in order to locate and inspect the same area in images recorded at different bias voltages. Features of type B are clearly visible at bias +1.5 V, but their contrast becomes weak below +1.0 V. On the other hand, the A features are clearly visible in a bias range from +0.5 to +1.5 V, whereas their contrast becomes much weaker at lower bias. The contrast at the left edge of the void also changes at different bias voltages, similar to what observed for the contrast of features A and B.

Figures 1(i) and 1(j) show STM and AFM images, respectively, of the area indicated by a square in Fig. 1(a). In both figures, the honeycomb lattice structure of graphene is clearly visible also within the A and B features, indicating that these features do not correspond to defects of the graphene lattice itself or to adsorbates on graphene. Moreover, point defects in graphene would result in a clear electronic signature, which is obviously absent in this case [21–23]. The AFM image in Fig. 1(j) shows a darker contrast at the positions of the A and B features, i.e., a more negative $\Delta f$ compared with the surrounding flat area. In addition, the lateral extension of feature B is larger than that of feature A.

These qualitative observations can be quantified by analyzing the cross-sectional profiles extracted from the STM data. Figures 2(a) and 2(b) show line profiles of typical A and B features at various bias voltages. Their apparent height varies with the bias voltage. The A features have a brighter appearance than the B ones in the range of bias voltage from +1.5 to +0.1 V; however, at –0.05 V they appear darker with respect to the B features and also to the surrounding flat area. Figure 2(c) shows line profiles extracted from the AFM image in Fig. 1(j), taken along the [11$\bar{2}$0] direction.

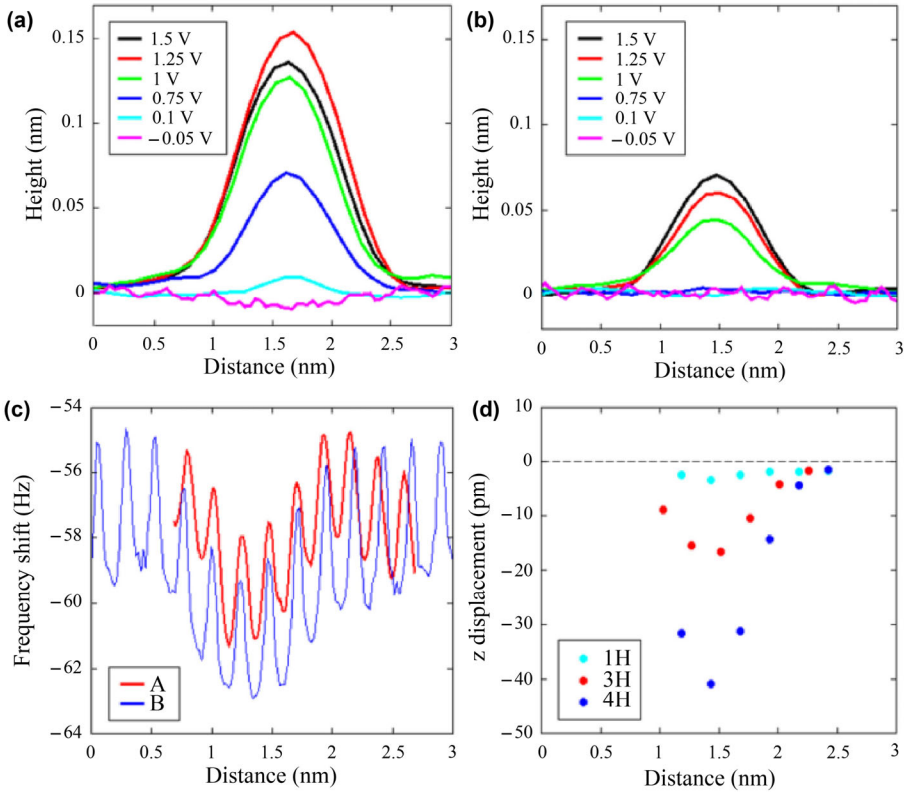


**Figure 2** Line profiles of features A (a) and B (b) observed in the STM images recorded at various bias voltages and with a tunneling current of 5 pA. (c) Line profiles of features A and B indicated by the red and blue lines along the [11$\bar{2}$0] direction in the AFM image shown in Fig. 1(j). The images were taken at a $T$ = 5 K. (d) DFT-calculated vertical displacement of C atoms along the [11$\bar{2}$0] direction for vacancies with one (cyan), three (red), and four (blue) missing H atoms.

These profiles show that $\Delta f$ is more negative at the feature positions than in the surrounding flat area. In addition, both the lateral extension and the extent of frequency decrease are larger for feature B than for feature A. Any decrease in frequency corresponds to an increased tip-sample distance and, as we are operating the AFM in constant-height mode, it indicates a depression of the surface morphology [24, 25]. Therefore, these data imply that, at the positions of the features, graphene is deformed towards the substrate, and the depression is more pronounced in the case of the B features. The possibility that an atom or a cluster larger than H was intercalated at the positions corresponding to the features can be excluded, because in that case graphene would be deformed towards the vacuum, rather than towards the substrate.

This general picture was confirmed by the DFT calculations. We evaluated the structure and electronic properties of several vacancies with a different number of missing H atoms, from 1 to 13 (see the ESM for details of the corresponding calculations). The results of this extensive sampling are reported elsewhere [26]. All modeled structures display intrusions of the graphene sheet towards the substrate, and the depth of these intrusions increases with the size of the vacancy. Figure 2(d) reports the $z$ displacement of C atoms along the [11$\bar{2}$0] direction, for three selected cases of vacancies with one, three, and four missing atoms (1H, 3H, and 4H, also illustrated in Fig. 4). The 1H vacancy displays a very small (a few pm) inward bending, which would be barely detectable by AFM [25]; similarly, the 2H vacancies display almost negligible inward bending of less than 5 pm (not shown in the figure). The 3H and 4H vacancies appear as the only ones compatible with the experimental observations, being the smallest with a detectable bending (between 20 and 40 pm), while larger vacancies display inward displacements of more than 50–60 pm, which is likely to be much larger than the observed range. The simulated AFM images generated from charge density isosurfaces are shown in the third row of Fig. 4. In agreement with the experimental observations, the images of the 3H and 4H vacancies show low and high contrast, respectively, while the 1H vacancy is almost undetectable. We stress that these calculations were performed in almost neutral conditions because the DFT calculations do not accurately reproduce the natural doping of QFMLG. This is mainly due to the poor representation of the substrate, as reported elsewhere [26]. Furthermore, an artificially-induced doping, introduced by positively charging graphene, might increase the inward bending because the positive charge localizes under the vacancies. However, in the case of 1H vacancies a detectable bending was only observed for doping levels at least three times larger than in the experiment.

STS measurements were performed to characterize the electronic states of the two types of features. Figures 3(a) and 3(b) show the STS curves corresponding to the two features and to the surrounding flat area. Each curve was obtained by averaging over 20 spectra recorded from different features of the same type. All three curves show a gap with a width of approximately 0.1 V at around 0 V, and a dip at +0.25 V, see Fig. 3(a). The gap-like feature was already observed in STS measurements of graphene [27]. This feature was attributed to the suppression of electronic tunneling to graphene states with a large wave vector near the Fermi energy and to the simultaneous enhancement of electronic tunneling at higher energy owing to a phonon-mediated inelastic channel. The dip at +0.25 V corresponds to the energy position of the Dirac point. Subtracting the energy of the out-of-plane acoustic graphene phonon mode (67 mV), the Dirac point is located 0.18 eV above the Fermi energy, indicating p-type doping in graphene with a hole concentration of $2 \times 10^{12}$ cm$^{-2}$. This is in good agreement with previous experimental and theoretical reports on similar samples [28].

The gap and the dip features are not resolved in the wide-range spectra shown in Fig. 3(b), owing to the larger tip-sample distance for these measurements (see figure caption). However, the spectra recorded for features A and B show an additional peak at +1.1 and +1.4 V, respectively, which is absent in the spectrum of the flat area. This observation is statistically significant, as shown by the histogram in Fig. S1(b) in the ESM. The peak energies for features A and B are qualitatively consistent with their contrast in the STM images. Assuming that the energy dependence of the density of states (DOS) of the tip and of the tunneling transmissivity is negligible, the tunneling

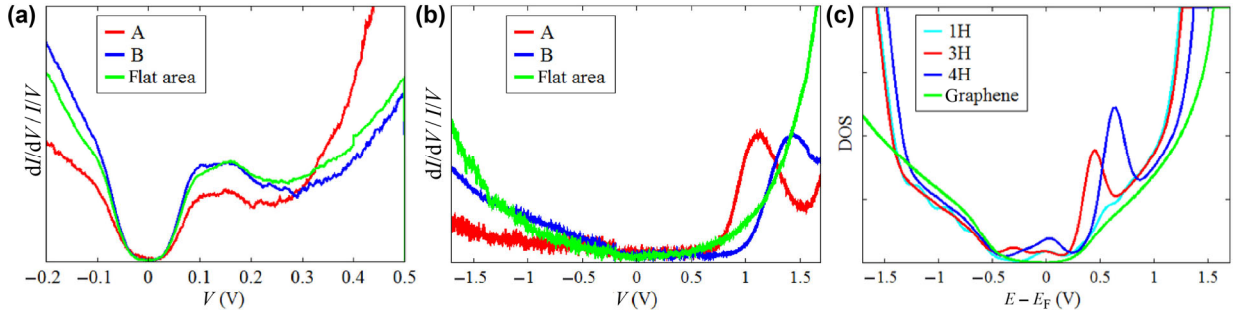


**Figure 3** (a) and (b) STS curves recorded for the A and B features and for a flat area. The energy range is (a) –0.2 to +0.5 V and (b) –1.7 to +1.7 V. The measurements were performed at $T$ = 5 K, with $V_{stab}$ = 0.5 (a) and 1.7 V (b), and $I_{stab}$ = 0.01 nA for both (a) and (b). (c) Calculated DOS for vacancies with one, three, and four missing hydrogen atoms and for free graphene. See text for details.

current is proportional to the integral of the density of states of the sample from the Fermi energy to the bias voltage. In constant-current mode, a feedback retracts the tip from the sample as the tunnel current increases. Therefore, the image contrast becomes brighter at the positions where the integrated density of states is larger. The integral of the STS curves in Fig. 3(b), calculated from the Fermi energy to any voltage above the onset of peak A (+0.75 V), is larger for peak A than for peak B, since the peak energy of A is lower than that of B, and their peak intensities are almost the same. This is consistent with the fact that the STM contrast for bias voltages above +0.75 V is brighter for the A than for the B features.

## 4 Discussion

The inverse photoemission spectra showed that the buffer layer possesses a state located 1.1 eV above the Fermi energy, associated with Si dangling bonds, which disappears after H intercalation [29]. The STS curves for graphene on the C-face of SiC (SiC(000$\bar{1}$)) also showed similar peaks [30]. This surface also exhibits Si dangling bonds at the interface. Peak energies of +1.4 and +1.6 V were obtained at two special positions within the unit cell, termed hollow and top sites, respectively, in which the Si dangling bonds are located at the center of a graphene hexagon and on top of a graphene C atom [30]. In the case of the present QFMLG, the observed differences between the electronic states of the two types of features may also be attributed to different local graphene–Si stacking configurations.

The STS data can be interpreted based on the calculated DOS of models containing different types of vacancies. The DOS curves of all examined systems share a common feature, consisting of a partially filled peak localized across the Fermi level. We verified that in all cases this is an electronic state localized on the vacancy between the two layers, corresponding to a dangling bond (see the second row of Fig. 4). For all vacancies with more than one missing H, a second (empty) peak appears in the STS curve, whose energy increases with the size of the vacancy. This peak corresponds to an electronic state still localized at the vacancy but with different symmetry, protruding slightly more upwards and with an electronic density interfering with that of the π system of graphene. The total DOS curves for vacancies 1H, 3H, and 4H are reported in the ESM. In order to compare the calculated DOS to the STS measurements, two aspects must be considered.

The first is that we have approximated the local STS measurements as the DOS calculated over the whole cell. However, our calculations are performed on a supercell including only a few layers of the substrate and whose lateral size is only slightly larger (at most double) than the extension of the vacancy itself. Therefore, the present calculations already represent an "almost-local" measurement with resolution similar to the experimental one. In fact, local DOS calculations performed by integrating volumes smaller than the simulation cell show only a slight increase in the relative weight of the DOS of the localized state with respect to that of graphene, along with a similar small increase in the relative weight of

the empty peak with respect to the filled one, with no overall improvement in the agreement with the experimental data.

However, this is unlikely to be the main source of difference between the DOS and STS data. The already-discussed gap-like feature at the Fermi level implies a suppression and masking of the filled peak, which is consequently not visible in the STS measurement. We mimic this effect by using a smoothing switch function to suppress the DOS around the Fermi level.

The corrected DOS curves, aligned to the Fermi level, are reported in Fig. 3(c). As can be seen, the 1H vacancy peak almost completely disappears, while the 3H and 4H vacancies display unoccupied peaks at energies above the Fermi level. Their energy location is somewhat lower than in the experiment, which is a common issue associated with the evaluation of excited states by DFT. However, the relative location and displacement of the peaks are reproduced, which strongly supports our assignment of peak A to the 3H vacancy and peak B to the 4H vacancy. We verified (data reported elsewhere [26]) that the DOS is almost independent of the relative translation of the graphene lattice with respect to the vacancy. The DOS curves of 1H vacancies located on hollow and top positions of the graphene lattice are basically indistinguishable from each other, and the same also holds for the possible different 3H and 4H vacancies with different translations. Therefore, the difference between the A and B features is unlikely to arise from the different location of the corresponding vacancy. This is not in contrast with the above-mentioned results for the C-face of SiC [30], because in that case the Si dangling bond is much closer to the graphene sheet than in the case of the present QFMLG, for which the exact location of the single vacant Si site is of minor importance. It should be noted that even for the most inwardly bent case, i.e., the 4H vacancy, Si atoms do not form covalent bonds with graphene. Their dangling bonds thus act as charged scattering centers for charge transport in QFMLG.

The complex voltage-dependence of the A- and B-type vacancies can be explained based on the nature of these states. The STS peaks (corresponding to empty states in the theoretical DOS) can be described as antibonding states, whose electronic density interferes with the $\pi$ system and protrudes outwards with respect to the graphene sheet. Therefore, they are visible as bright features at the bias voltages corresponding to the peaks. This is supported by the simulated STM images reported in the fourth row of Fig. 4.

Because the peaks are located at different energies, the maximum brightness appears at different voltages, causing variable contrast. As the location of the peaks differs in the theoretical and experimental measurements, one cannot use the experimental voltage values for the evaluation of STM images. Therefore, the STM images were evaluated at different voltages, in each case fully including the empty peak and excluding the filled one, which is not visible in the experiment. The brightness of the vacancies is similar, but, as noted above, it was evaluated at different voltages. The 1H vacancy does not show appreciable contrast, because its DOS is located at the Fermi level, and therefore not visible in the STM experiment.

In addition, we observe that the electronic state protrusion is somewhat counterbalanced by the structural intrusion. While the latter is constant, the former is voltage-dependent. Therefore, at a given voltage (away from the peak) the contrast can switch to negative. The switch happens at different voltages for A and B features, because the structural intrusion and the location/size of the peaks are different.

## 5 Conclusions

The present AFM and STM measurements support the assignment of the A and B features to smaller and larger vacancies, respectively. In particular, the 3H- and 4H-type vacancies, respectively, are the most consistent with the experimental data for the A and B features. Even in the most inward-bent case, i.e., the 4H vacancy, the Si atoms do not form covalent bonds with graphene, but keep their dangling bonds, which degrade the charge carrier mobility of QFMLG.

Furthermore, this study demonstrates that a combination of STM/AFM and DFT is an ideal tool to evaluate the distribution, size, and electronic structure of atomic-size defects. Using these techniques, we have probed the interactions between graphene and

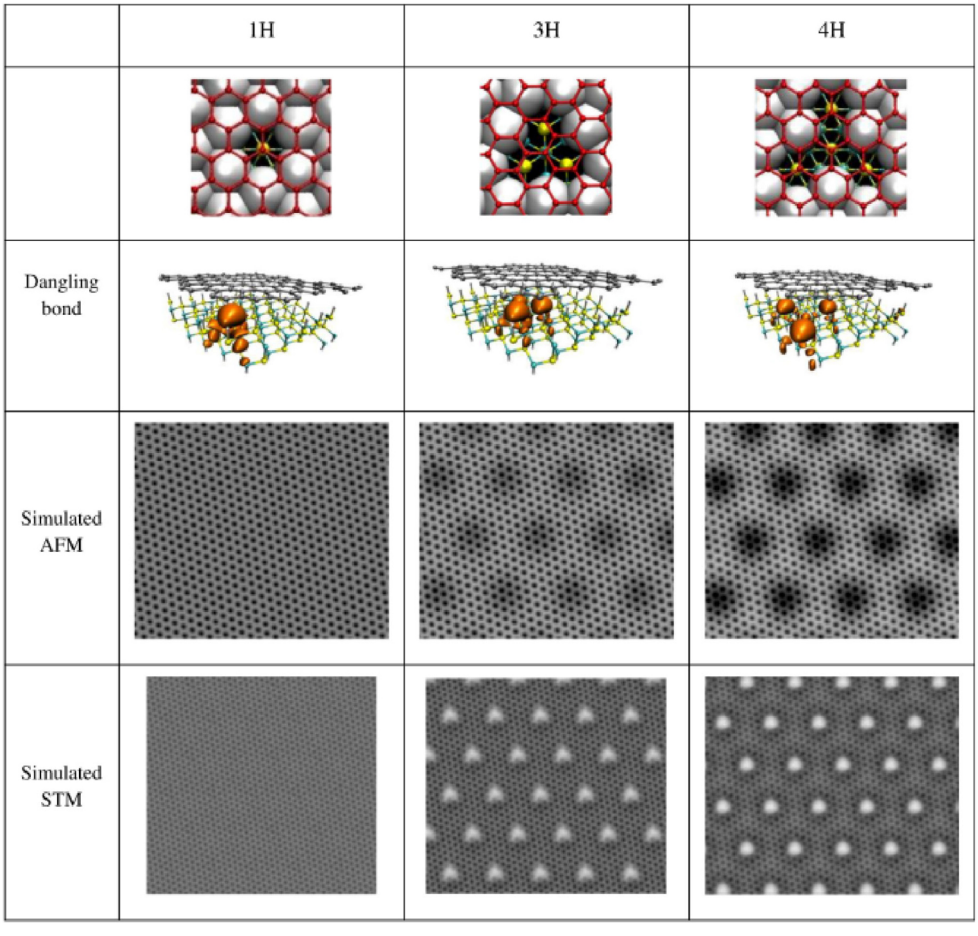


**Figure 4** Theoretical analysis of the structure of vacancies with one, three, and four missing H atoms (columns 1H, 3H, 4H). The fully relaxed structure models of the vacancies are represented in the first row, where the graphene lattice, Si, and substrate C atoms are colored red, yellow, and cyan, respectively, whereas H atoms are represented as white enlarged spheres to highlight the vacancies. The following data are shown in the subsequent rows for each type of vacancy: an isosurface representation of the dangling bond state localized between graphene and SiC; the simulated AFM images (obtained from the total electron density represented on a horizontal plane located between the tip and graphene, see the ESM for details); the simulated isocurrent STM images, calculated at voltages fully including the empty peak and excluding the filled one. The STM images are obtained as constant-density ($10^{-6}$ e·Å$^{-3}$) isosurfaces of the dangling bond state, color-coded according to the height (see the ESM for details). The periodicity is imposed by the model system and approximately corresponds to a completely occupied 6 × 6 superlattice.

SiC. The atomic and electronic structures of charge-scattering centers in QFMLG were revealed in high detail for the first time, using both experimental and theoretical data. Our results provide new insight into the relevant defects in QFMLG and might be useful for determining the lowest free-energy configuration of this material. This will support the optimization of the synthesis conditions of QFMLG, such as the substrate temperature, duration, and pressure for the H intercalation process, in order to reduce the density of Si dangling bonds. Therefore, the present work provides the detailed understanding required for the rational design of high-mobility QFMLG. Moreover, the approach illustrated in this study can be applied to investigate localized states in other systems, such as graphene interfaces intercalated with different elements.

## Acknowledgements

We acknowledge travel support from COST Action MP1103 "Nanostructured materials for solid-state hydrogen storage". Funding from the European Union Seventh Framework Program under Grant

Agreement No. 696656 Graphene Flagship Core1 is also acknowledged. Financial support from the CNR in the framework of the agreements on scientific collaborations between CNR and CNRS (France), NRF (Republic of Korea), and RFBR (Russia) is acknowledged. We also thank the European Research Council (ERC) for funding under the European Union's Horizon 2020 research and innovation program (No. 670173), the ERC Advanced Grant CEMAS (No. 291194), the ERC Consolidator Grant AMSEL (No. 682144), the EU project PAMS (No. 610446), and the Initial Training Network QTea (No. 317485), and Scuola Normale Superiore for support via the internal project SNS16_B_HEUN – 004155. Furthermore, we acknowledge funding from the Italian Ministry of Foreign Affairs. We gratefully acknowledge CINECA for providing HPC resources under the ISCRA-C grants "Quasi-free-standing graphene monolayer on SiC with H-coverage vacancies: a density functional theory study" (2016–2017) and "Electro-mechanical manipulation of graphene" (2015–2016), and for technical support.

**Electronic Supplementary Material**: Supplementary material (histogram analysis of the A and B features, further details on the model system and the calculation setup, and on the total DOS calculations) is available in the online version of this article at https://doi.org/10.1007/s12274-017-1697-x.



## References

[1] Bolotin, K. I.; Sikes, K. J.; Jiang, Z.; Klima, M.; Fudenberg, G.; Hone, J.; Kim, P.; Stormer, H. L. Ultrahigh electron mobility in suspended graphene. *Solid State Commun.* **2008**, *146*, 351–355.

[2] Goler, S.; Coletti, C.; Piazza, V.; Pingue, P.; Colangelo, F.; Pellegrini, V.; Emtsev, K. V.; Forti, S.; Starke, U.; Beltram, F.; Heun, S. Revealing the atomic structure of the buffer layer between SiC (0001) and epitaxial graphene. *Carbon* **2013**, *51*, 249–254.

[3] Riedl, C.; Coletti, C.; Iwasaki, T.; Zakharov, A. A.; Starke, U. Quasi-free-standing epitaxial graphene on SiC obtained by hydrogen intercalation. *Phys. Rev. Lett.* **2009**, *103*, 246804.

[4] Bocquet, F. C.; Bisson, R.; Themlin, J.-M.; Layet, J.-M.; Angot, T. Reversible hydrogenation of deuterium-intercalated quasi-free-standing graphene on SiC(0001). *Phys. Rev. B* **2012**, *85*, 201401.

[5] Speck, F.; Jobst, J.; Fromm, F.; Ostler, M.; Waldmann, D.; Hundhausen, M.; Weber, H. B.; Seyller, T. The quasi-free-standing nature of graphene on H-saturated SiC(0001). *Appl. Phys. Lett.* **2011**, *99*, 122106.

[6] Ciuk, T.; Caban, P.; Strupinski, W. Charge carrier concentration and offset voltage in quasi-free-standing monolayer chemical vapor deposition graphene on SiC. *Carbon* **2016**, *101*, 431–438.

[7] Forti, S.; Emtsev, K. V.; Coletti, C.; Zakharov, A. A.; Riedl, C.; Starke, U. Large-area homogeneous quasifree standing epitaxial graphene on SiC(0001): Electronic and structural characterization. *Phys. Rev. B* **2011**, *84*, 125449.

[8] Murata, Y.; Mashoff, T.; Takamura, M.; Tanabe, S.; Hibino, H.; Beltram, F.; Heun, S. Correlation between morphology and transport properties of quasi-free-standing monolayer graphene. *Appl. Phys. Lett.* **2014**, *105*, 221604.

[9] Sclauzero, G.; Pasquarello, A. Intercalation of H at the graphene/SiC(0001) interface: Structure and stability from first principles. *Appl. Surf. Sci.* **2014**, *291*, 64–68.

[10] Deretzis, I.; La Magna, A. Interaction between hydrogen flux and carbon monolayer on SiC(0001): Graphene formation kinetics. *Nanoscale* **2013**, *5*, 671–680.

[11] Yamasue, K.; Fukidome, H.; Funakubo, K.; Suemitsu, M.; Cho, Y. Interfacial charge states in graphene on SiC studied by noncontact scanning nonlinear dielectric potentiometry. *Phys. Rev. Lett.* **2015**, *114*, 226103.

[12] Tanabe, S.; Takamura, M.; Harada, Y.; Kageshima, H.; Hibino, H. Effects of hydrogen intercalation on transport properties of quasi-free-standing monolayer graphene. *Jpn. J. Appl. Phys.* **2014**, *53*, 04EN01.

[13] Giessibl, F. J. High-speed force sensor for force microscopy and profilometry utilizing a quartz tuning fork. *Appl. Phys. Lett.* **1998**, *73*, 3956–3958.

[14] Giessibl, F. J. Advances in atomic force microscopy. *Rev. Mod. Phys.* **2003**, *75*, 949–983.

[15] Albrecht, T. R.; Grütter, P.; Horne, D.; Rugar, D. Frequency modulation detection using high-*Q* cantilevers for enhanced force microscope sensitivity. *J. Appl. Phys.* **1991**, *69*, 668–673.

[16] Giannozzi, P.; Baroni, S.; Bonini, N.; Calandra, M.; Car, R.; Cavazzoni, C.; Ceresoli, D.; Chiarotti, G. L.; Cococcioni, M.; Dabo, I. et al. QUANTUM ESPRESSO: A modular and open-source software project for quantum simulations of materials. *J. Phys. Condens. Matter* **2009**, *21*, 395502.

[17] Cavallucci, T.; Tozzini, V. Multistable rippling of graphene on SiC: A density functional theory study. *J. Phys. Chem. C* **2016**, *120*, 7670–7677.

[18] Rappe, A. M.; Rabe, K. M.; Kaxiras, E.; Joannopoulos, J. D. Optimized pseudopotentials. *Phys. Rev. B* **1990**, *41*, 1227–1230.

[19] Perdew, J. P.; Burke, K.; Ernzerhof, M. Generalized gradient approximation made simple. *Phys. Rev. Lett.* **1996**, *77*, 3865–3868.

[20] Grimme, S. Semiempirical GGA-type density functional constructed with a long-range dispersion correction. *J. Comput. Chem.* **2006**, *27*, 1787–1799.

[21] Ugeda, M. M.; Fernández-Torre, D.; Brihuega, I.; Pou, P.; Martínez-Galera, A. J.; Pérez, R.; Gómez-Rodríguez, J. M. Point defects on graphene on metals. *Phys. Rev. Lett.* **2011**, *107*, 116803.

[22] Ugeda, M. M.; Brihuega, I.; Hiebel, F.; Mallet, P.; Veuillen, J.-Y.; Gómez-Rodríguez, J. M.; Ynduráin, F. Electronic and structural characterization of divacancies in irradiated graphene. *Phys. Rev. B* **2012**, *85*, 121402.

[23] Mashoff, T.; Convertino, D.; Miseikis, V.; Coletti, C.; Piazza, V.; Tozzini, V.; Beltram, F.; Heun, S. Increasing the active surface of titanium islands on graphene by nitrogen sputtering. *Appl. Phys. Lett.* **2015**, *106*, 083901.

[24] Boneschanscher, M. P.; van der Lit, J.; Sun, Z. X.; Swart, I.; Liljeroth, P.; Vanmaekelbergh, D. Quantitative atomic resolution force imaging on epitaxial graphene with reactive and nonreactive AFM probes. *ACS Nano* **2012**, *6*, 10216–10221.

[25] Schuler, B.; Liu, W.; Tkatchenko, A.; Moll, N.; Meyer, G.; Mistry, A.; Fox, D.; Gross, L. Adsorption geometry determination of single molecules by atomic force microscopy. *Phys. Rev. Lett.* **2013**, *111*, 106103.

[26] Cavallucci, T.; Murata, Y.; Heun, S.; Tozzini, V. H-coverage defects in quasi free standing graphenemonolayer on SiC: A density functional theory study. in preparation.

[27] Zhang, Y. B.; Brar, V. W.; Wang, F.; Girit, C.; Yayon, Y.; Panlasigui, M.; Zettl, A.; Crommie, M. F. Giant phonon-induced conductance in scanning tunnelling spectroscopy of gate-tunable graphene. *Nat. Phys.* **2008**, *4*, 627–630.

[28] Sławińska, J.; Aramberri, H.; Muñoz, M. C.; Cerdá, J. I. *Ab initio* study of the relationship between spontaneous polarization and p-type doping in quasi-freestanding graphene on H-passivated SiC surfaces. *Carbon* **2015**, *93*, 88–104.

[29] Lin, Y. P.; Ksari, Y.; Themlin, J. M. Hydrogenation of the buffer-layer graphene on 6H-SiC (0001): A possible route for the engineering of graphene-based devices. *Nano Res.* **2015**, *8*, 839–850.

[30] Hiebel, F.; Mallet, P.; Veuillen, J. Y.; Magaud, L. Impact of local stacking on the graphene–impurity interaction: Theory and experiments. *Phys. Rev. B* **2012**, *86*, 205421.